Microchimica Acta (2025) 192:241
https://doi.org/10.1007/s00604-025-06988-3

RESEARCH

Visualization of protrusion-localized *STAT3* mRNA using a self-powered lipidic nanoflare for predicting hepatocellular carcinoma metastasis

Ya Zhang[2,3] · Ruichao Zeng[1] · Yuanhang Xia[1] · Wei Han[4] · Yifei Luan[5] · Yuheng Zhang[1] · Shijia Wu[2,3] · Shouhao Wang[2,3] · Jinyong Wang[2,3] · Yongping Chen[2,3] · Dazhi Chen[1,2]

Received: 10 October 2024 / Accepted: 15 January 2025 / Published online: 18 March 2025

Abstract

Cancer cell metastasis is one of the major causes of patients death with hepatocellular carcinoma (HCC). Previous findings demonstrated that protrusion-accumulated *STAT3* mRNA is highly related to HCC cell metastasis, making protrusion-localized *STAT3* mRNA an ideal biomarker for evaluating HCC cell initiation and progression. A self-powered lipidic nanoflare (SLNF) has been developed for detecting the expression level of protrusion-accumulated *STAT3* mRNA in individual HCC cells, which enables accurate prediction of HCC metastasis. The LNF system is a cholesterol micelle decorated with two kinds of DNA probes, a double-stranded response DNA and a single-stranded fuel probe. The cholesterol micelle can be easily assembled from an amphipathic cholesterol-conjugated DNA via hydrophobicity-mediated aggregation, exhibiting a highly efficient cell internalization. Moreover, the compact and high-density arrangement of DNA probes on the surface of cholesterol micelle enhances their biostability. All the above features make the LNF system an ideal approach for intracellular RNA imaging. The assay commences with the binding of *STAT3* mRNA to the response DNA, which peels off the waste DNA and exposes the toehold domain. This domain serves as the proximal holding point for the fuel probe to initiate a strand displacement amplification, which is a crucial step in enabling the detection of targets expressed at trace levels, yielding a limit of detection (LOD) of 100 pM at 37 °C within 1.5 h. The SLNF system is expected to provide useful insight into the development of simple and degradation-resistant DNA probes for visual prediction of HCC metastasis, showing potential applications in tumor diagnosis and treatment.

Keywords Protrusion-localized *STAT3* mRNA · Lipidic nanoflare · Hepatocellular carcinoma metastasis · DNA nanotechnology · Cell imaging

Introduction

Tumor metastasis is the major cause of the death of cancer patients [1, 2]. Cancer cell motility makes a significant contribution to the process of cancer metastasis [3, 4]. The formation of cell protrusions at the leading edge is closely

Ya Zhang and Ruichao Zeng contributed equally to this study.

✉ Yongping Chen
cyp@wmu.edu.cn

✉ Dazhi Chen
dazhichen@hmc.edu.cn

[1] School of Clinical Medicine, The First People's Hospital of Lin'an Distract, Hangzhou, Lin'an People's Hospital Affiliated to Hangzhou Medical College, Hangzhou Medical College, Hangzhou 310053, China

[2] Hepatology Diagnosis and Treatment Center, The First Affiliated Hospital of Wenzhou Medical University & Zhejiang Provincial Key Laboratory for Accurate Diagnosis and Treatment of Chronic Liver Diseases, Wenzhou 325035, China

[3] Hepatology Institute of Wenzhou Medical University, Wenzhou 325035, China

[4] Center of Laboratory Animal, Hangzhou Medical College, Hangzhou 310053, China

[5] School of Innovation and Entrepreneurship, Hangzhou Medical College, Hangzhou 310053, China

associated with tumor migration and invasion, which are critical for tumor metastasis [5, 6]. As highly polarized structures, cell protrusions are rich in various proteins, signaling factors, and nucleic acids that are responsible for cellular polarity and directed migration [6–8]. Recently, researchers discovered that specific mRNAs can be enriched in the protrusions of metastatic cancer cell lines and play an important role in the transcription and enrichment of corresponding protein products [9]. For example, *STAT3* mRNA accumulates in the protrusions by interacting with FMRP [10], an RNA-binding protein. Increasing research evidences have demonstrated that FMRP modulates the localization, stability, and translation of *STAT3* mRNA, which facilitates the metastasis of hepatocellular carcinoma (HCC) [11, 12]. Accordingly, it is significant to develop practical detection technologies that are capable of reliably testing *STAT3* mRNA for evaluating the initiation and development of HCC cells.

There are various methods for predicting the metastasis of hepatocellular carcinoma (HCC). Commonly used methods include imaging examinations, such as ultrasound, computed tomography (CT), and magnetic resonance imaging (MRI), which have limited sensitivity and detection capabilities for early-stage lesions [13, 14]. Tissue biopsy is an invasive method, and during the biopsy process, tumor cells may spread along the wound, increasing the risk of intrahepatic metastasis [14]. For deep learning and multi-omics approaches, the results depend on the quality of the data, and biases in the data can lead to misleading outcomes [15].

Currently, DNA nanomaterials, due to their biocompatibility, programmability, and strong addressability, have been widely applied. For example, Chen et al. [16] published a study using DNA aptamers to selectively identify highly metastatic liver cancer cells, and through magnetic nanoparticle modification, they achieved screening and detection. This method has high specificity and is suitable for molecular detection of early metastasis. However, the stability of aptamers needs further study, and the adaptability to different HCC subtypes is not yet fully clear. Wu et al. [17] designed DNA probes to bind with microRNAs related to liver cancer, amplifying Raman scattering signals for ultra-sensitive detection. Although this method achieved multi-channel detection of multiple microRNAs with sensitivity reaching the attomolar (aM) level, it relies on high-cost equipment and complex nanomaterial preparation. In contrast, the self-powered lipidic nanoflare (SLNF) system is low-cost and simple, and it has the capability for intracellular imaging, providing spatial information on *STAT3* mRNA expression in living cells. This offers a highly sensitive and specific tool for predicting HCC metastasis.

When it comes to mRNA detection, typical tools are real-time polymerase chain reaction (RT-PCR) [18], microarray analysis [19], and northern blots [20]. Despite their frequent application over the last decades, these approaches are hampered by time and sample consumption, making them unsuitable for mRNA imaging in real-time and detecting cell-to-cell variations. To acquire the spatial information of mRNA expression in living cells, there is a pressing need for the development of cell imaging technologies. Fluorescence in situ hybridization (FISH), a classic approach for RNA detection in tissue and cells, has proven a pivotal method to promote the development of cell imaging [21]. However, current methods of FISH still have their drawbacks. Significant challenges are the low sensitivity and compromised specificity [21, 22]. These limitations create difficulties in detecting genes such as mRNA with very low expression levels and differentiating their various mutations. Therefore, there is a significant need for developing novel methodologies that enable ultrasensitive and highly selective detection of mRNA in living cells.

Recently, DNA cascade circuits, such as hybridization chain reaction (HCR) and catalytic hairpin assembly (CHA), have been widely applied in RNA detection and imaging that take advantage of their enzyme-free process and highly effective signal amplification [23]. For example, Wang's group [24] once reported a catalytic DNA circuit based on CHA for intracellular RNA imaging with a high sensitivity. Li's group [25] reported an enzymatically gated CHA for the tumor-specific activation of signal amplification in RNA imaging. These strategies rely on the DNA cascade circuits to achieve an efficient nonenzymatic signal amplification. Although important progress has been achieved, conventional DNA cascade circuits with single- and double-stranded DNA hairpins are fragile under a cellular environment, resulting in high false positive signals, which have been recognized as a major barrier in DNA nanotechnology. To address this issue, novel detecting systems with high nuclease resistance have been reported [26]. Among them, DNA nanoflares are proven powerful tools for cell imaging because of their remarkable cell permeability and high DNA biostability [27, 28]. Oligonucleotide probe-functionalized gold nanoparticles (AuNP), for instance, are typical DNA nanoflares [29, 30]. However, the DNA loading based on Au–S bond is inefficient and the additional requirement of salt-aging protocol generally takes a few days.

It is worth noting that cholesterol-conjugated DNA strands (Chol-DNA) have drawn widespread attention in the construction of DNA spherical micelles for biomedical applications due to their inherent high-efficiency assembly and facile operation [31, 32]. Chol-DNA is an attractive amphiphilic molecule consisting of a hydrophobic cholesterol, a TEG linker, and a hydrophilic DNA [33, 34]. The DNA spherical micelles can be assembled from Chol-DNA via hydrophobicity-mediated aggregation by simple stirring in a buffered solution [34, 35]. The DNA spherical micelles

have emerged as the potential substitute for oligonucleotide-functionalized AuNPs.

Taking the above points into consideration, we developed a simple yet efficient self-powered lipidic nanoflare (SLNF) for visualizing protrusion-localized *STAT3* mRNA and predicting hepatocellular carcinoma metastasis. We demonstrated that SLNF possesses several advantages, such as high sensitivity and low false positive signal, making it a practical biosensor under cellular conditions. The final intracellular assays yielded ultrasensitive and reliable results for evaluating the initiation and development of HCC cells. We believe that the SLNF system provides a reliable method for biomedical imaging and diagnosis.

Experimental method

Preparation of the SLNF system

Construction of DNA spherical micelle

Chol-DNA (2 μL, 10 μM) was diluted with 2 μL of 10 × PBS (1370 mmol/L NaCl, 27 mmol/L KCl, 100 mmol/L Na_2HPO_4, 20 mmol/L KH_2PO_4, pH 7.4) to a concentration of 5 μM. The mixture was then heated to 95 °C for 5 min and then gradually cooled to room temperature.

Assembly of double-stranded response DNA

The assembly of double-stranded response DNA was executed by mixing an equal amount (1 μL, 10 μM) of DNA1, DNA2, and Linker strand, followed by diluting with ddH_2O to reach a final volume of 20 μL.

Assembly of the SLNF system

The assembly of the SLNF system was executed by mixing double-stranded response DNA (20 μL) and fuel probes (1 μL) with DNA spherical micelle (4 μL), followed by diluting with ddH_2O to reach a final volume of 25 μL. After incubation at 37 °C for 1 h, the SLNF system was constructed and then stored at 4 °C before further use.

Fluorescent measurement

The SLNF system (25 μL) was prepared as previously mentioned above. The *STAT3*-responsive assay was conducted by adding 0.5 μL and 10 μM of *STAT3* mRNA and incubating it at 37 °C for 1 h. The reaction mixture was then diluted with 1 × PBS to a final volume of 200 μL, and the fluorescence was scanned using a Hitachi F-7000 fluorescence spectrometer (Hitachi, Ltd., Japan). The excitation wavelength was set at 492 nm, and the fluorescence emission spectra were recorded from 500 to 600 nm. Specially, we used DNA oligonucleotides as proxies for mRNA, because RNA is more susceptible to degradation by RNases, which are ubiquitous in the environment and biological samples.

Gel electrophoresis

Samples for gel electrophoresis were prepared by mixing 8 μL of the reaction mixture, 2 μL of SYBR Green I, and 2 μL of 6 × loading buffer. Native polyacrylamide gel electrophoresis (nPAGE, 12%) was performed using 0.5 × TBE (4.5 mM Tris, 4.5 mM boric acid, 0.1 mM EDTA, pH 7.9) as the working buffer under a constant voltage of 90 V for 50 min. The gel was visualized and analyzed by employing a GelDoc Go imaging system (Bio-Rad, USA).

DLS measurement

A 25 μL SLNF system was prepared as described above, the sample was diluted to 100 μL using ddH2O, and its diameter was tested using the Litesizer 500 (AntonPaar).

TEM imaging

The SLNF system (25 μL) was prepared as described above, and 10 μL was dropped onto the TEM microgrid and incubated for 30 min. Excess liquid was removed with a pipette and allowed to dry overnight. TEM images were scanned the next day using a transmission electron microscope (TEM, 200 kV, JEM-F200).

Cell culture

HCCLM3 and A549 cells were cultured in DMEM with 10% fetal bovine serum (FBS) and 1% penicillin–streptomycin. HELF and MDA-MB231 cells were cultured in RPMI 1640 medium supplemented with 10% FBS and 1% penicillin–streptomycin. All of the above cells were incubated at 37 °C in 5% CO_2.

Cell imaging

Cells were first inoculated on a 0.17-mm thick cell slide in a 24-well plastic-bottom plate and incubated at 37 °C in 5% CO_2 for 24 h. SLNF system (100 μL) was diluted with the cell medium to a final concentration of 200 nM (reaction solution). After being washed three times with 1 × PBS, the cells were incubated with the reaction solution for 4 h. Subsequently, the cells were stained with 10 μL DAPI for 15 min and further washed three times with 1 × PBS. Cell imaging was performed using the confocal laser scanning microscope (Nikon).

Flow cytometry assay

All flow cytometry measurements were performed using Cytoflex (Beckman Coulter, Inc). HCCLM3 cells were seeded in 6-well plates and incubated overnight. After washing three times with 1 × PBS, 200 nM SLNF (600 µL per well) was added and incubated at 37 °C in the dark for the corresponding time. It was digested using 0.25% trypsin digestion solution (Beyotime Biotech Inc) and then washed three times with 1 × PBS before being tested on the machine.

Fluorescence in situ hybridization (FISH)

The fluorescent in situ hybridization kit was purchased from Guangzhou Ruibo Biotechnology Co., LTD (Guangzhou, China). The pre-hybridization solution was prepared according to the ratio of pre-hybridization to blocking buffer of 99:1 and incubated with the cell slide covered with cells for 30 min. Then *STAT3*-mRNA probe (20 µm) was added to the hybridization solution at the ratio of hybridization to buffer of 99:1 and incubated with the cell slide for 16 h. Imaging was performed the confocal laser scanning microscope (Nikon).

Quantitative polymerase chain reaction (qPCR)

To evaluate the *STAT3* mRNA expression levels in cells cultured as described above, total RNA was extracted from the cells using Trizol reagent. The HiScript III All-in-one RT SuperMix Perfect for qPCR kit and Taq Pro Universal SYBR qPCR Master Mix kit were purchased from Vazyme Biotech Co., Ltd (Nanjing, China). All the experimental procedures used followed the manufacturer's protocol. Thereafter, the RT-qPCR experimental data was analyzed by BIORADCF X96 software to appraise relative expression levels of *STAT3* mRNA in cells using the $2^{(-\Delta\Delta CT)}$ method.

Transwell assay

The 2.5×10^5 cells were seeded into the upper chamber of a polycarbonate transwell chamber (#3422, Corning, USA) with an 8-µm pore size with 200 µl medium without FBS. The chambers were then placed in the 700 µl medium with 18% FBS for 48 h to drive cell invasion. Cells in the lower chamber were fixed in 4% paraformaldehyde and stained with 1% crystal violet. Chambers were photographed, and the total migrated cells were quantified by Image J software.

Wound-healing assay

Cells were cultured in 6-well plates, a "wound" was created by the tip of a 200-µl pipette, and "healing" was monitored at the indicated time points. The closure area was quantified and the mobility was calculated using Image J software.

Results and discussion

Working principle of SLNF system and its application for cell viability assay

Because the protrusion-accumulated *STAT3* mRNA is highly related to the metastasis of hepatocellular carcinoma cells [12], making a protrusion-localized *STAT3* mRNA is an ideal biomarker for evaluating the initiation and development of HCC cells. Scheme 1A shows the *STAT3* mRNA imaging and cell viability assay by using the SLNF system. The SLNF system is a DNA spherical micelle decorated with two DNA components: a double-stranded response DNA and a single-stranded fuel DNA. The double-stranded response DNA is assembled from three DNA (DNA 1, DNA 2, and Linker strand), which results in two toeholds, toeholds 1 and 2. The single-stranded fuel DNA is a hairpin-shaped probe. The working principle of the SLNF system is shown in Scheme 1B. Specifically, the reaction starts with the binding of mRNA to toehold 1, and then DNA 1 can be peeled off during the strand displacement reaction. Because of this reaction, toehold 2 can be released. Then the exposed toehold 2 can be used as the adjacent holding point for fuel DNA to hybridize with the Linker strand, leading to the displacement of DNA 2 and mRNA. The released mRNA then goes on to initiate the next rounds of the reaction cycle to obtain a signal amplification. To obtain a high cell permeability and DNA biostability, the response DNA and fuel DNA are arranged on the surface of DNA spherical micelle. The micelle assembly relies on the hydrophobicity-mediated aggregation of an amphiphilic molecule, cholesterol-modified DNA strands (Chol-DNA). Chol-DNA consists of a hydrophobic cholesterol, a TEG linker, and a hydrophilic DNA. Details can be found in Fig. 1A. After loading on the surface of the spherical micelle, the biostability of DNA components can be remarkably enhanced according to the literature report. Similarly, the reaction cycle contains five steps: mRNA binding (Step I), release of DNA 1 (Step II), hybridization of fuel DNA with Linker strand (Step III), release of mRNA (Step IV), and triggering next reaction cycle by mRNA (Step V). DNA 1 and 2 are labeled with FAM and BHQ 1 for signaling, details can be found in Table S1.

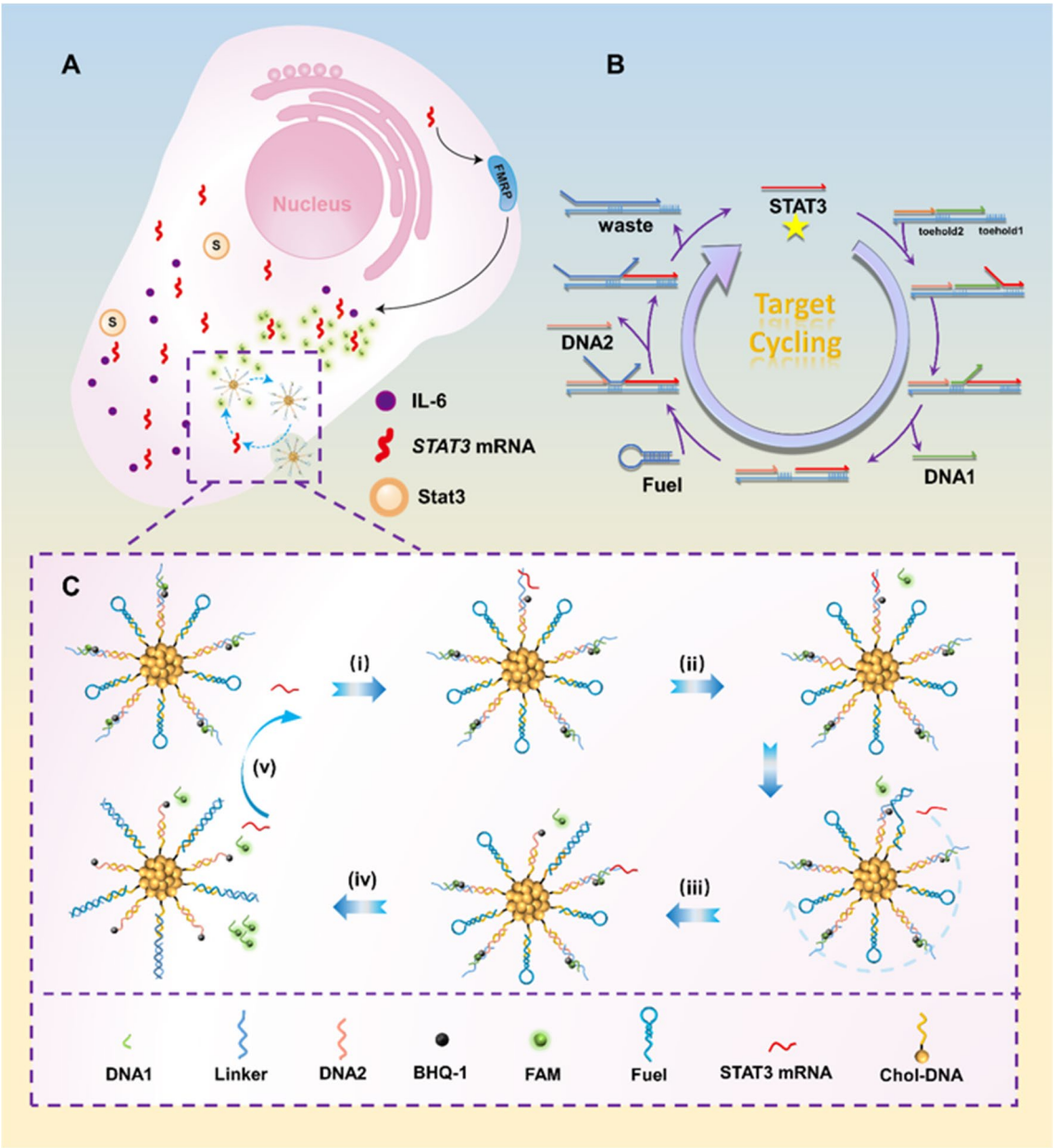

Scheme 1 Design of a self-powered lipidic nanoflare (SLNF) for visualizing protrusion-localized *STAT3* mRNA and predicting hepatocellular carcinoma metastasis. **A** Schematic illustration of the *STAT3* mRNA-initiated SLNF within living cells. **B** Working principle of the double-stranded response DNA and the single-stranded fuel DNA for amplified *STAT3* mRNA detection. **C** Schematic triggering of SLNF system consisting of a DNA spherical micelle, double-stranded response DNAs, and single-stranded fuel DNAs in the presence of *STAT3* mRNA

Feasibility of SLNF system

After elaborating on the working principle of the SLNF system, its application for mRNA detection was verified in vitro. As shown in Fig. 1B, the stepwise assembly of the SLNF system was validated by gel electrophoresis. Samples 1 to 3 represent DNA 1, the fuel probe, and the DNA spherical micelle, respectively. Samples 4 and 5 demonstrated that DNA 1 and the fuel probe can be connected on the surface of the DNA spherical micelle, supported by the disappearance of the band of DNA 1 and the fuel probe. Samples 6 to 9 show the successful assembly of the SLNF system by mixing the double-stranded response DNA and fuel probe with DNA spherical micelle, which is evidenced by the single band at the top. In addition, the stepwise assembly of double-stranded response DNA can be verified by the gradual slower-moving band (samples 1–7, Fig. S1).

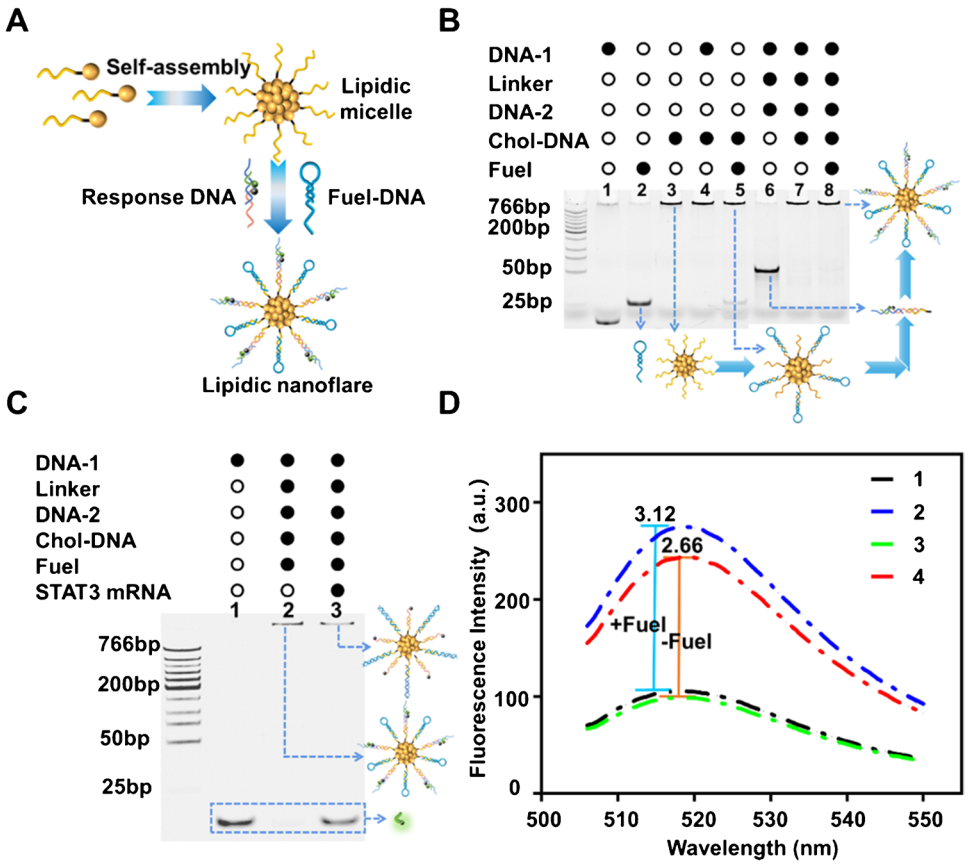

Fig. 1 Feasibility of the SLNF for *STAT3* mRNA detection. **A** Schematic diagram of the construction of DNA spherical micelle. **B** Native polyacrylamide gel electrophoresis nPAGE, 12% to confirm the stepwise assembly of the SLNF system. **C** Native polyacrylamide gel electrophoresis nPAGE, 12% to confirm the feasibility of SLNF system for *STAT3* mRNA detection. The filled circle and open circle in gel electrophoresis denote the presence and absence of the corresponding components, respectively. **D** Feasibility analysis by fluorescence spectra, (1) Chol-DNA + DNA1 + DNA 2 + Linker strand + Fuel probe, (2) Chol-DNA + DNA1 + DNA 2 + Linker strand + fuel probe + *STAT3* mRNA, (3) Chol-DNA + DNA1 + DNA 2 + Linker strand, (2) Chol-DNA + DNA1 + DNA 2 + Linker strand + *STAT3* mRNA

Then the application of the SLNF system for mRNA detection was verified by gel electrophoresis and fluorescence measurement. For gel electrophoresis, the strand displacement amplification was verified by the appearance of the FAM-labeled DNA 1 in sample 3 in Fig. 1C. For fluorescence measurement (Fig. 1D), a low fluorescence signal was detected in the absence of target mRNA (line 1), while a strong signal can be observed in the presence of target mRNA (line 2), resulting in a high signal-to-noise ratio (SNR = 3.12). On the contrary, the system shows a lower signal-to-noise ratio (SNR = 2.66) in the absence of a fuel probe (lines 3 and 4), verifying the working principle of strand displacement amplification in Scheme 1. It is worth noting that the lower background can be obtained by using a hairpin-shaped fuel probe. As shown in Fig. S2, if the fuel probe without a hairpin shape was used to assemble the SLNF system, a strong background signal was detected. Therefore, the above results demonstrated the feasibility of the SLNF system for amplified mRNA detection.

Performance evaluation for mRNA detection in vitro

In order to obtain the best performance of the SLNF system for amplified mRNA detection, the crucial experimental parameters were optimized, including the DNA sequences of the fuel probe and the reaction time. As shown in Fig. S3, the stem of the fuel probe with 16 bp was found to possess a lower background and higher response signal, and the optimal reaction time was 1.5 h. These parameters were used in the following experiments. Figure 2A shows the typical fluorescence spectra of the SLNF system when detecting target mRNA, the fluorescence signal increased with the increased concentration of target mRNA. The fluorescence spectra in the presence of a low concentration of the target are presented in the inset. The signal at 100 pM can be detected compared with the blank, which can be defined as the limit of detection (LOD). Figure 2B plots the peak fluorescence intensity in the presence of target mRNA at different concentrations. Two different dose–response curves can be observed and specifically presented in Fig. 2C and D. In the low concentration of target mRNA, the linear relationship is described as $F = 0.02525C + 61.37$ with a correlation coefficient (R^2) of 0.9969. In the high target concentration of target mRNA, the linear relationship is $F = 3.720C + 74.42$ with an R^2 of 0.9910. Among them, the symbols F and C represent the response signal of the SLNF system and the concentration of target mRNA, respectively.

Moreover, to verify the specificity of the SLNF system when detecting *STAT3* mRNA, other nontarget mRNAs were selected as the target analytes, including β-actin, GalNAc-T,

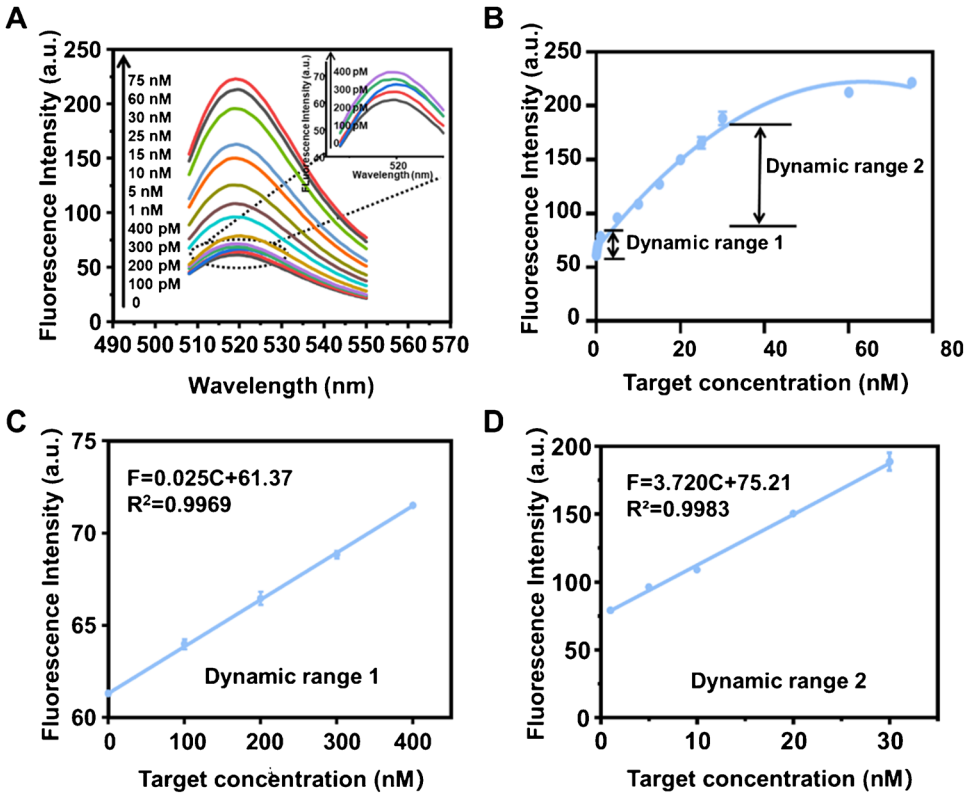

Fig. 2 The analytical performance of the SLNF system for *STAT3* mRNA detection. **A** Fluorescence spectra of the SLNF system in the presence of different target concentrations ranging from 0 to 100 nM. Inset: fluorescence spectra of targets at low target concentrations. **B** Dependence of the peak fluorescence intensity response from (**A**). Linear response of the sensing system in the range of **C** low and **D** high concentrations of target STAT 3 mRNA. The error bar represents means ± SD ($n = 3$)

Survivin, Craf-1, and C-myc. As shown in Fig. S4, the strong signal can be detected only present with the target *STAT3* mRNA, while less than 10% signal can be observed when detecting other nontarget mRNA if defining the signal of miR-21 as 100%, indicating the high specificity of SLNF system for detecting *STAT3* mRNA.

Biostability of SLNF system

Because of the complicated cellular environment, the practical application of DNA probes is hampered by their intrinsic susceptibility to extracellular and intracellular nuclease degradation, which has been considered one of the major technical problems in DNA nanotechnology [36–38]. To address this issue, chemical modification is often applied to DNA molecules [39, 40]. However, the cost of mRNA detection will increase dramatically. Moreover, cytotoxicity from the chemical reagent generated additional difficulties in the clinical application. In this work, the SLNF system is a desirable approach for operating under physiological environments. Because the compact and high-density DNA was reported with a higher biostability according to the literature report, in the SLNF system, the compact and high-density arrangement of DNA probes on the surface of cholesterol micelle enhances their biostability. To verify this, the serum stability of the SLNF system was evaluated by incubating with FBS according to the typical method. As shown in Fig. S5A, the SLNF system is compatible with 10% FBS for at least 24 h, as evidenced by most of the DNA bands (about 80%) being remnant. On the contrary, the double-stranded response DNA was rapidly attenuated to 40% after incubating with 10% FBS (Fig. S5B). In addition, the performance of the SLNF system was also evaluated in different concentrations of FBS. As shown in Fig. S5C, fluorescence intensities of the SLNF system with and without the target in FBS were almost the same as that in the buffered solution (FBS = 0%). And the signal-to-ratio of the SLNF system exhibited a negligible change (Fig. S5D). These results demonstrated that the SLNF system possesses a high serum stability and low false-positive signal, making the SLNF system suitable for operating in physiological sets.

Capability of the SLNF system to quantify mRNA in individual cells

Encouraged by the promising performance in vitro, we applied the SLNF system to detect *STAT3* mRNA in living cells. The cytotoxicity of the SLNF system was evaluated using a CCK-8 kit by incubating with HCCLM3, A549, and HLEF cells. Negligible cytotoxicity was observed in Fig. S6, indicating great potential for application in living cells. Before cell imaging, optimization experiments showed that the optimal reaction time (Fig. S7) and probe concentration (Fig. S8) were 4 h and 200 nM, which were

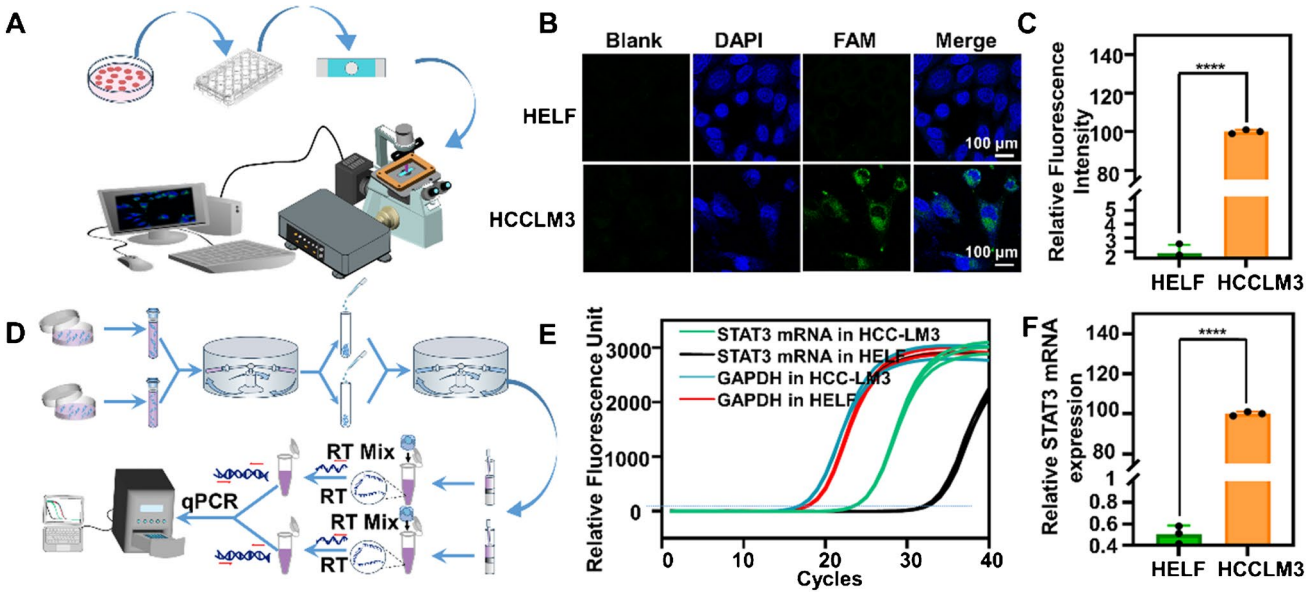

Fig. 3 The SLNF system and PCR were used to detect *STAT3* mRNA expression in HCCLM3 and HELF cells. **A** Schematic diagram of cell culture and confocal imaging steps. **B** CLSM images of HCCLM3 and HELF cells after incubating with the SLNF system. Scale bars = 100 μm. **C** The quantitative analysis of relative FAM signal of the CLSM images by Image J software. **D** Schematic diagram of RNA extraction and qPCR procedures. To transfer cells from the petri dishes to centrifuge tubes, clean them with 1 × PBS and extract the RNA within the cells then prepare the reagent mixture required for reverse transcription (RT mix), and reverse transcription was conducted using a qPCR instrument. The resulting ctDNA can be directly utilized for qPCR. **E** qPCR curves of *STAT3* mRNA and GAPDH extracted from HCCLM3 and HELF cells. **F** Statistical analysis of relative expression levels of *STAT3* mRNA in HCCLM3 and HELF cells. The error bar represents the means ± SD ($n = 3$). ****$p < 0.0001$, independent sample *t*-test

chosen for subsequent cell experiments. Then we applied the SLNF system to detect *STAT3* mRNA by using confocal laser scanning microscopy (CLSM) in HCCLM3, a characteristic metastatic HCC cell line. Normal cells (HELF) were used as the control. Figure 3A shows the program flow diagram of the SLNF system for *STAT3* mRNA imaging. As shown in Fig. 3B, the fluorescence signal cannot be observed in HELF cells, while a strong signal was detected in HCCLM3. Figure 3C shows the quantitative result of the cells in Fig. 3B. Moreover, the *STAT3* mRNA expression level in the two different cells was analyzed by quantitative polymerase chain reaction (qPCR) according to the program flow diagram shown in Fig. 3D. Figure 3E and F shows the curve and quantitative result of qPCR. One can see that the CLSM images by the SLNF system are in good agreement with the *STAT3* mRNA expression levels estimated by the qPCR method, indicating the SLNF system provided an accurate result for detecting intracellular mRNA. To verify the sensitivity, we compared the SLNF system with FISH, a FAM-labeled single-stranded DNA probe (Fig. 4A). As shown in Fig. 4B, the fluorescence signal cannot be observed in HELF cells after incubating with the SLNF system or FISH. As shown in the confocal images (Fig. 4C) and quantitative analysis (Fig. 4D), *STAT3* mRNA was barely detected by FISH but can be easily detected by the SLNF system, indicating that the SLNF system offers significantly better sensitivity. SLNF system was also applied to detect *STAT3* mRNA in different cancer cells, MDA-MB-231, and HCCLM3 cells. As shown in Fig. S9, the difference in *STAT3* mRNA expression levels can be observed by incubating with the SLNF system.

Evaluating tumor metastasis by SLNF system

The more exciting result was that the protrusion-localized *STAT3* mRNA could be observed after incubating the SLNF system with HCCLM3 cells (Fig. S9). Then we applied the SLNF system to evaluate the tumor metastasis of HCC cells by detecting the expression level of protrusion-localized *STAT3* mRNA. Napabucasin, a novel *STAT3* inhibitor, suppresses proliferation, invasion, and stemness. The HCCLM3 cells were first pretreated with different Napabucasin (0, 5, 10 μM) for 48 h to inhibit the *STAT3* expression level. As shown in the wound-healing assay in Fig. 5A and quantitative analysis in Fig. 5B, a gradually decreased migration rate was observed. In addition, a transwell experiment (Fig. 5C) was also performed to evaluate the HCCLM3 cells pretreated with different Napabucasin. As shown in the result of the transwell experiment in Fig. 5D and quantitative analysis in Fig. 5E, the migration and invasion abilities of HCCLM3 cells decrease with increasing concentrations of Napabucasin. The above

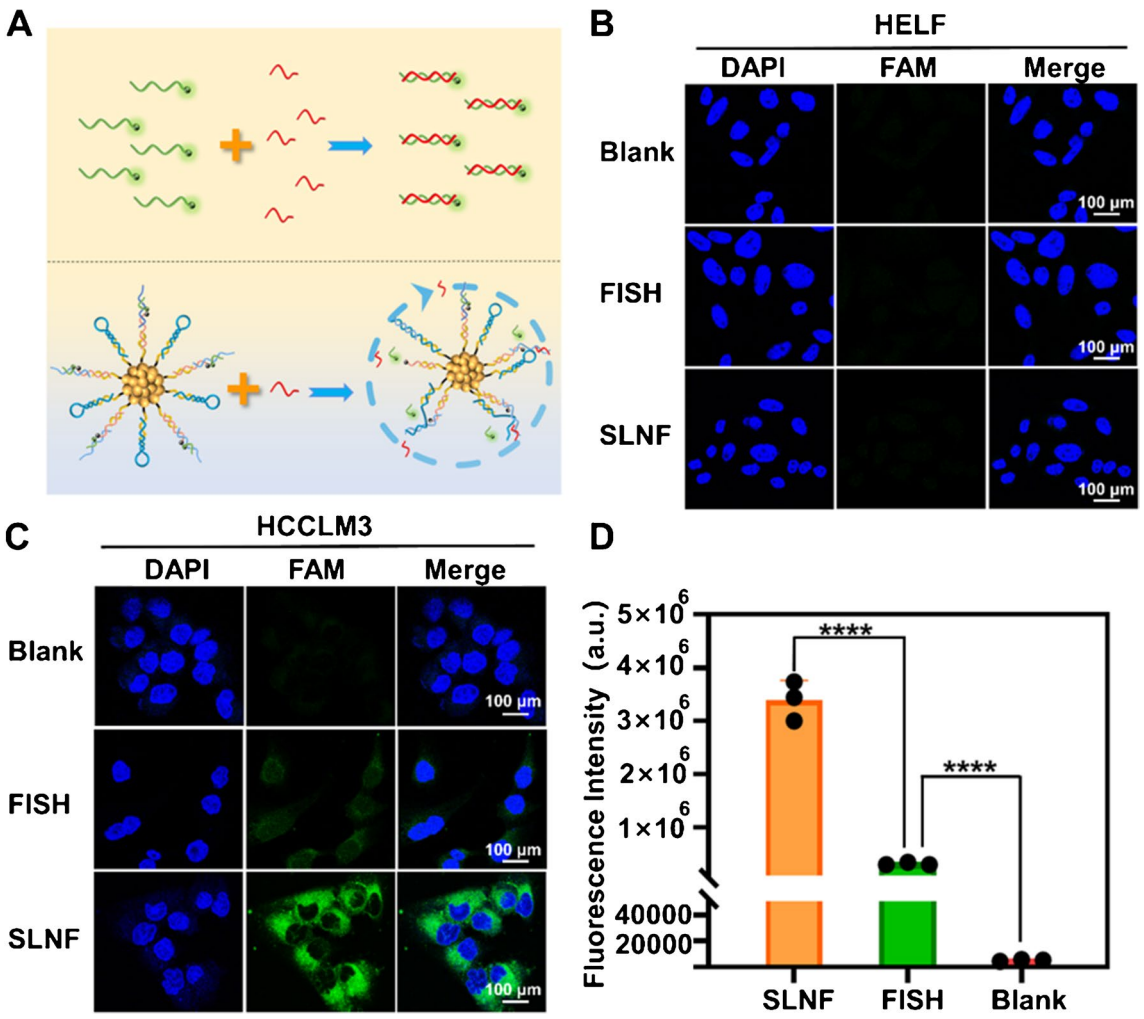

Fig. 4 Comparative imaging of *STAT3* mRNA imaging in HCCLM3 and HELF cells using fluorescence in situ hybridization (FISH) and SLNF system. **A** Schematic diagram of the molecular mechanism of two detection systems. CLSM images of HELF **B** and HCCLM3 **C** cells after incubating with FISH or SLNF system. **D** Systematic statistical analysis of the relative fluorescence intensity of HCCLM3 cells in (**C**). The error bar represents the means ± SD ($n = 3$). ****$p < 0.0001$, independent sample *t*-test

results demonstrated that the migration and invasion abilities of HCCLM3 cells can be inhibited by incubating with Napabucasin. Then the Napabucasin-pretreated HCCLM3 cells were further incubated with the SLNF system. As shown in Fig. 5F, the fluorescence intensities in cytoplasm and protrusion decrease with the increasing concentrations of Napabucasin. Figure 5G shows the quantitative analysis of the fluorescence signal in protrusion, the protrusion-located *STAT3* mRNA expression level decreases in the order of cells pretreated with 0, 5, and 10 μM of Napabucasin. Taking together, the above results show that the fluorescence signal and the migration and invasion abilities of HCCLM3 cells exhibit positive correlations, indicating that hepatocellular carcinoma metastasis can be predicted by the SLNF system.

Conclusion

We developed a simple and efficient self-powered lipidic nanoflare (SLNF) for detecting the expression level of protrusion-accumulated *STAT3* mRNA in individual HCC cells. The compact and high-density arrangement of DNA probes on the surface of cholesterol micelle improves their biostability in complex physiological environments. We demonstrated that the SLNF system was compatible with 10% FBS for at least 12 h and exhibits a low false positive signal. The strand displacement amplification in the SLNF system can be operated on the surface of cholesterol micelle, yielding a limit of detection (LOD) of 100 pM at 37 °C within 1.5 h. The application for *STAT3* mRNA

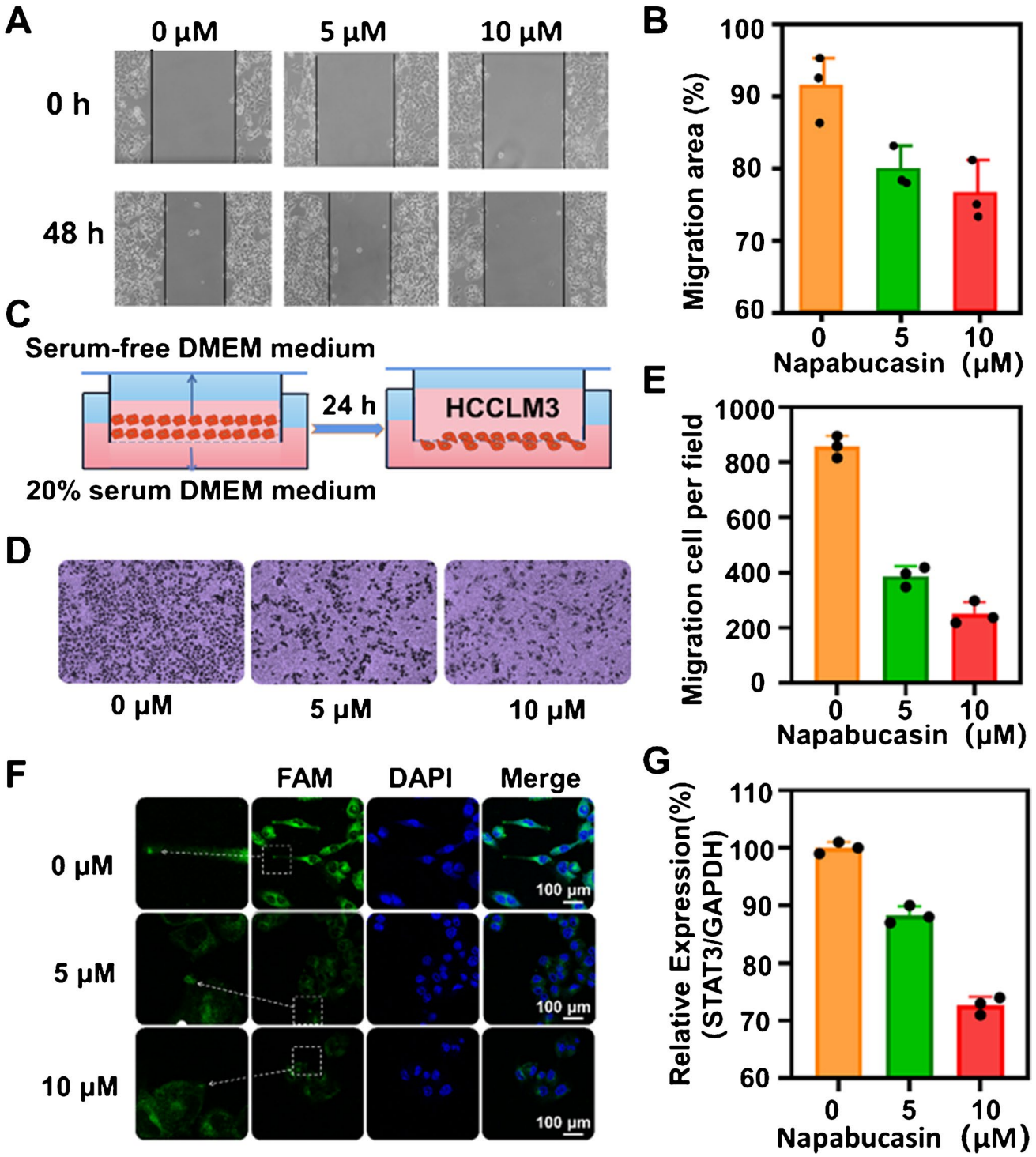

Fig. 5 **A** Evaluation of the migration ability of HCCLM3 cells treated with different concentrations of Napabucasin by wound-healing assay. **B** Quantification analysis of wound-healing assay by Image J software. **C** Schematic evaluating HCCLM3 cell migration by using the Transwell experiment. **D** The migration and invasion abilities of HCCLM3 cells treated with different concentrations of Napabucasin using Transwell assay. **E** Statistical analysis of the number of HCCLM3 cells passing through the membrane after 48 h. **F** CLSM images of HCCLM3 cells after treated with different concentrations of Napabucasin. Scale bars = 100 μm. **G** The quantitative analysis of the CLSM images in (**F**) by Image J software. The error bar represents the means ± SD ($n = 3$)

in serum samples was also verified, indicating a powerful molecular tool for biomedical diagnostics. In addition, the SLNF system shows a low cytotoxicity and a high cell internalization, making the system suitable for cell imaging. Comparative analysis illustrates that the proposed system is superior to the classic fluorescence in situ hybridization (FISH) method. Final applications for evaluating the initiation and development of HCC cells can be achieved by detecting protrusion-localized *STAT3* mRNA. In this work, the SLNF system may open new avenues for designing practical DNA probes for predicting hepatocellular carcinoma metastasis and showing potential applications for tumor diagnosis and treatment.

Supplementary Information The online version contains supplementary material available at https://doi.org/10.1007/s00604-025-06988-3.

Author contribution Y. Z. and R Z. Responsible for methodology, data management, software, and validation. Y. X., W. H., and Y. L. are responsible for data organization, investigation, validation, and software. Y. Z. and S W. Responsible for methodology, investigation, and software. S. W. and J W. Responsible for software and validation. Y. C. and D C. Responsible for conceptualization, resource allocation, funding acquisition, writing reviews, and editing. All authors have reviewed the manuscript.

Funding This work was supported by the Young Scientists Fund of the National Natural Science Foundation of China (grant number: 82200632) and Major Project From Basic Scientific Research Funds, Hangzhou Medical College (grant number: KYZD202201).

Data availability No datasets were generated or analysed during the current study.

Declarations

Competing interests The authors declare no competing interests.

References

1. Ganesh K, Massagué J (2021) Targeting metastatic cancer. Nat Med 27:34–44
2. Steeg PS (2006) Tumor metastasis: mechanistic insights and clinical challenges. Nat Med 12:895–904
3. Weiss L, Ward PM (1983) Cell detachment and metastasis. Cancer Metastasis Rev 2:111–127
4. Zanotelli MR, Zhang J, Reinhart-King CA (2021) Mechanoresponsive metabolism in cancer cell migration and metastasis. Cell Metab 33:1307–1321
5. Eddy RJ, Weidmann MD, Sharma VP, Condeelis JS (2017) Tumor cell invadopodia: invasive protrusions that orchestrate metastasis. Trends Cell Biol 27:595–607
6. Nazari SS, Doyle AD, Bleck CKE, Yamada KM (2023) Long prehensile protrusions can facilitate cancer cell invasion through the basement membrane. Cells 12. https://doi.org/10.3390/cells12202474
7. Deborde S, Omelchenko T, Lyubchik A, Zhou Y, He S, McNamara WF et al (2016) Schwann cells induce cancer cell dispersion and invasion. J Clin Invest 126:1538–1554
8. Yang D, Qu F, Cai H, Chuang CH, Lim JS, Jahchan N et al (2019) Axon-like protrusions promote small cell lung cancer migration and metastasis. Elife 8. https://doi.org/10.7554/eLife.50616
9. Cai W, Ji J, Wu B, Hao K, Ren P, Jin Y et al (2021) Characterization of the small RNA transcriptomes of cell protrusions and cell bodies of highly metastatic hepatocellular carcinoma cells via RNA sequencing. Oncol Lett 22:568
10. Shen Z, Liu B, Wu B, Zhou H, Wang X, Cao J et al (2021) FMRP regulates STAT3 mRNA localization to cellular protrusions and local translation to promote hepatocellular carcinoma metastasis. Commun Biol 4. https://doi.org/10.1038/s42003-021-02071-8
11. Zhao X, Yang J, Zhang J, Wang X, Chen L, Zhang C, Shen Z (2022) Inhibitory effect of aptamer-carbon dot nanomaterial-siRNA complex on the metastasis of hepatocellular carcinoma cells by interfering with FMRP. Eur J Pharm Biopharm 174:47–55
12. Liu Y-H, Jin J-L, Wang Y-Z, Tan Y, Zhou Y-Y, Peng T et al (2016) Protrusion-localized STAT3 mRNA promotes metastasis of highly metastatic hepatocellular carcinoma cells in vitro. Acta Pharmacol Sin 37:805–813
13. Budhu A, Forgues M, Ye QH, Jia HL, He P, Zanetti KA et al (2006) Prediction of venous metastases, recurrence, and prognosis in hepatocellular carcinoma based on a unique immune response signature of the liver microenvironment. Cancer Cell 10:99–111
14. Chan YT, Zhang C, Wu J, Lu P, Xu L, Yuan H et al (2024) Biomarkers for diagnosis and therapeutic options in hepatocellular carcinoma. Mol Cancer 23:189
15. Huang Y, Fang F, Liu L, Chen K, Du Y (2024) Prediction of drug targets related to HCC metastasis from the perspective of programmed cell death based on transformer. Futur Gener Comput Syst 160:918–925
16. Chen H, Yuan CH, Yang YF, Yin CQ, Guan Q, Wang FB, Tu JC (2016) Subtractive cell-SELEX selection of DNA aptamers binding specifically and selectively to hepatocellular carcinoma cells with high metastatic potential. Biomed Res Int 2016:5735869
17. Wu J, Zhou X, Li P, Lin X, Wang J, Hu Z et al (2021) Ultrasensitive and simultaneous SERS detection of multiplex MicroRNA using fractal gold nanotags for early diagnosis and prognosis of hepatocellular carcinoma. Anal Chem 93:8799–8809
18. Kilic T, Erdem A, Ozsoz M, Carrara S (2018) microRNA biosensors: opportunities and challenges among conventional and commercially available techniques. Biosens Bioelectron 99:525–546
19. EkizKanik F, Celebi I, Sevenler D, Tanriverdi K, LortlarÜnlü N, Freedman JE, Ünlü MS (2022) Attomolar sensitivity microRNA detection using real-time digital microarrays. Sci Rep 12:16220
20. Blevins T (2010) Northern blotting techniques for small RNAs. Methods Mol Biol 631:87–107
21. Gozzetti A, Le Beau MM (2000) Fluorescence in situ hybridization: uses and limitations. Semin Hematol 37:320–333

22. Fox JL, Hsu PH, Legator MS, Morrison LE, Seelig SA (1995) Fluorescence in situ hybridization: powerful molecular tool for cancer prognosis. Clin Chem 41:1554–1559
23. Fu T, Lyu Y, Liu H, Peng R, Zhang X, Ye M, Tan W (2018) DNA-based dynamic reaction networks. Trends Biochem Sci 43:547–560
24. Xie C, Li R, Gong X, Zhang Q, Zhang Y, Wang Z et al (2023) Efficient intracellular microRNA imaging based on the localized and self-sustainable catalytic DNA assembly circuit. Anal Chem 95:10398–10404
25. Zhang M, Zhang Y, Zhang X, Liu K, Li L, Yu Z et al (2024) An enzymatically activated and catalytic hairpin assembly-driven intelligent AND-gated DNA network for tumor molecular imaging. Anal Chem 96:10084–10091
26. Whitfield CJ, Zhang M, Winterwerber P, Wu Y, Ng DYW, Weil T (2021) Functional DNA-polymer conjugates. Chem Rev 121:11030–11084
27. Seferos DS, Giljohann DA, Hill HD, Prigodich AE, Mirkin CA (2007) Nano-flares: probes for transfection and mRNA detection in living cells. J Am Chem Soc 129:15477–15479
28. Chen M, Duan R, Xu S, Duan Z, Yuan Q, Xia F, Huang F (2021) Photoactivated DNA walker based on DNA nanoflares for signal-amplified MicroRNA imaging in single living cells. Anal Chem 93:16264–16272
29. He X, Zeng T, Li Z, Wang G, Ma N (2016) Catalytic molecular imaging of microRNA in living cells by DNA-programmed nanoparticle disassembly. Angew Chem Int Ed Engl 55:3073–3076
30. Cao X, Ye Y, Liu S (2011) Gold nanoparticle-based signal amplification for biosensing. Anal Biochem 417:1–16
31. Tenchov R, Bird R, Curtze AE, Zhou Q (2021) Lipid nanoparticles─from liposomes to mRNA vaccine delivery, a landscape of research diversity and advancement. ACS Nano 15:16982–17015
32. Yin H, Wang H, Li Z, Shu D, Guo P (2019) RNA Micelles for the systemic delivery of anti-miRNA for cancer targeting and inhibition without ligand. ACS Nano 13:706–717
33. Xue C, Wang L, Huang H, Wang R, Yuan P, Wu ZS (2021) Stimuli-induced upgrade of nuclease-resistant DNA nanostructure composed of a single molecular beacon for detecting mutant genes. ACS Sens 6:4029–4037
34. Li C, Xue G, Wu R, Zhang J, Cheng Y, Huang G et al (2024) Lighting up lipidic nanoflares with self-powered and multivalent 3D DNA rolling motors for high-efficiency MicroRNA sensing in serum and living cells. ACS Appl Mater Interfaces 16:281–291
35. Zhai F, Guan Y, Zhu B, Chen S, He R (2021) Intraparticle and interparticle transferable DNA walker supported by DNA micelles for rapid detection of microRNA. Anal Chem 93:12346–12352
36. Chandrasekaran AR (2021) Nuclease resistance of DNA nanostructures. Nat Rev Chem 5:225–239
37. Xue C, Zhang S, Yu X, Hu S, Lu Y, Wu ZS (2020) Periodically ordered, nuclease-resistant DNA nanowires decorated with cell-specific aptamers as selective theranostic agents. Angew Chem Int Ed Engl 59:17540–17547
38. Chen YJ, Groves B, Muscat RA, Seelig G (2015) DNA nanotechnology from the test tube to the cell. Nat Nanotechnol 10:748–760
39. Kabza AM, Kundu N, Zhong W, Sczepanski JT (2022) Integration of chemically modified nucleotides with DNA strand displacement reactions for applications in living systems. Wiley Interdiscip Rev Nanomed Nanobiotechnol 14:e1743
40. Wang Q, Chen X, Li X, Song D, Yang J, Yu H, Li Z (2020) 2′-fluoroarabinonucleic acid nanostructures as stable carriers for cellular delivery in the strongly acidic environment. ACS Appl Mater Interfaces 12:53592–53597